IEEE Access
Multidisciplinary ⋮ Rapid Review ⋮ Open Access Journal

Received May 4, 2021, accepted May 18, 2021, date of publication May 26, 2021, date of current version June 4, 2021.

Digital Object Identifier 10.1109/ACCESS.2021.3083918

Hybrid Approach for Vehicle Trajectory Prediction Using Weighted Integration of Multiple Models

GIHOON KIM[1], DONGCHAN KIM[1], YOONYONG AHN[2], AND KUNSOO HUH[1], (Member, IEEE)

[1]Department of Automotive Engineering, Hanyang University, Seoul 04763, South Korea
[2]Department of Automotive Engineering (Automotive-Computer Convergence), Hanyang University, Seoul 04763, South Korea

Corresponding author: Kunsoo Huh (khuh2@hanyang.ac.kr)

This work was supported by the Industrial Strategic Technology Development Program, Development and Evaluation of Automated Driving Systems for Motorway and City Road, funded by the Ministry of Trade, Industry Energy (MOTIE), South Korea, under Grant 10079730.

ABSTRACT Prediction of surrounding vehicles accurately is an essential prerequisite for safe autonomous driving. Trajectory prediction methods can be classified into physics-, maneuver-, or learning-based methods. Learning-based methods have been studied extensively in recent years because it effectively exploits the road information and interactions among vehicles. However, learning-based methods perform poorly in unseen environments that were not considered during training and provide unreasonable results such as inconsistent trajectories according to road geometry. In this paper, to address this problem, a hybrid model that combines a learning-based model with physics- and maneuver-based models according to their uncertainties is proposed. The deep ensemble technique is also used to estimate the uncertainty of the learning-based method. Because the deep ensemble tends to show a large variance in unseen environments, this method is used to determine whether to use a hybrid model. The proposed method is trained and validated using the Lyft l5 dataset, the real environment vehicle driving data containing several types of intersections.

INDEX TERMS Trajectory prediction, physics-based model, maneuver-based model, deep ensemble, uncertainty, weighted integrated model.

I. INTRODUCTION

Rapid advances have been made in Advanced driver assistance systems (ADAS) over several years, and systems such as adaptive cruise control (ACC) and lane keeping assistance (LKA), have already been effected in mass-produced vehicles. Nonetheless, systems, such as collision avoidance (CA), are still being developed to reduce accidents in general driving situations. In order to ensure safety, trajectory prediction is a key component of these systems.

Traditionally, physics- and maneuver-based methods are used for trajectory prediction. Physics-based methods estimate future trajectories using vehicle kinematic and dynamic models [1]–[4]. The dynamic models consider forces that affect the vehicle's movement such as the tire force. In contrast, the kinematic models do not consider such forces; rather, they exploit the mathematical relationship among velocity, position, and etc. Trajectory prediction using these models is typically performed using a filtering algorithm. In [5], [6], they predicted trajectories using Kalman filter with specific model, and multiple models were combined based on variances using Interacting Multiple Models in [7], [8]. Although the physics-based model is accurate for the short term, it is unreliable for long-term prediction. Furthermore, it does not effectively account for deceleration or acceleration caused by the surrounding vehicles and environment.

Maneuver-based methods, which entail maneuver recognition and trajectory prediction, have been proposed to improve the long-term prediction accuracy. Maneuver recognition identifies the driver's intentions from the vehicle state and environment, and trajectory prediction is performed based on the estimated maneuver. A maneuver is defined as a combination of longitudinal and lateral motions along a road lane in [9], [10]. It is selected according to the cost-to-go

The associate editor coordinating the review of this manuscript and approving it for publication was Ganesh Naik.

function, and the trajectory is planned in the longitudinal and lateral directions, respectively. Schreier *et al.* [11] made more detailed maneuver by considering information about the surrounding vehicles and roads. The maneuver is determined through the Bayesian network, and there are different motion models for each maneuver. Because the future trajectory in the maneuver-based method is predicted based on the road geometry, short- and long-term accuracy can be ensured by integrating it with the physics-based methods [12].

Recently, with the emergence of various deep learning techniques, learning-based trajectory prediction have been actively researched. Learning-based methods, compared to maneuver- and physics-based methods, make it relatively easier to consider road shape information and interactions among vehicles. Learning-based trajectory prediction methods can be divided according to the type of input. When using a top-view image over time as input [13], [14], all the components in the image can be automatically considered without additional processing. When using vectorized inputs, such as positions, velocities and lane boundaries [15]–[17], accurate values can be used without loss of information. Other researchers have used attention or graph neural networks to investigate the interactions among vehicles [18]–[21].

However, using only the learning-based method for trajectory prediction in an actual driving environment can cause problems. When driving in a new environment that was not observed during training, or when the density of surrounding vehicles changes, the deep learning network may receive input data with a different distribution from the training data. This increase the likelihood of the network predicting an unexpected future trajectory, which can lead to accidents due to undesirable planning. In recent years, learning-based and traditional methods have been combined [22], [23]. However, because they used traditional method only to identify maneuvers, the problem of predicting an unexpected trajectory remains unsolved.

In this study, an integrated model that combines the trajectory results from physics-, maneuver-, and learning-based method is proposed to improve trajectory prediction performance in various environments. Each model predicts the mean and variance at each time step; thus, predictions takes the form of a Gaussian function. Then, the trajectories predicted by the three models are integrated according to the inverse of the uncertainties. Because the median probability of the Gaussian distribution is inversely proportional to the variance, this method can be considered as a probability product for trajectory integration. The contributions of the study are as follows.

- The proposed model integrates physics-, maneuver-, and learning-based models based on the uncertainty of each model. This model improves the prediction performance by assigning greater weights to models with relatively less uncertainty.
- The proposed method can significantly reduce the unreasonable path prediction that may occur in unseen environments when using only learning-based methods. The deep ensemble method is utilized to tackle new environments by estimating the uncertainty of the learning-based model.
- Performance evaluation is conducted on the Lyft l5 dataset, which is not only collected under real-world vehicle driving conditions, but also includes various road environments such as intersections.

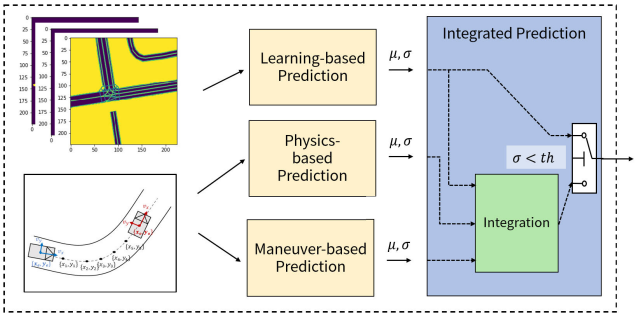

FIGURE 1. Overall system architecture.

II. SYSTEM OVERVIEW

The architecture of the overall system is shown in Fig.1. The system comprises prediction and integration modules. In the prediction module, the physics-, maneuver-, and learning-based models predict future trajectory positions (μ_x, μ_y) and their uncertainties (σ_x, σ_y) using the map and the history information of each vehicle. In the learning-based method, the deep ensemble technique is used to estimate the uncertainty. Detailed descriptions of each model are provided in Section III. The integration module first determines the model to be used based on the size of the uncertainty from the learning-based model. If the uncertainty is below a certain threshold, the integrated module takes the output of the learning-based model directly as a future trajectory. Otherwise, the future trajectory is replaced by a combination of the predicted trajectory and the uncertainty from each model. The combination method is discussed more detail in Section IV. In this study, the problem of predicting surrounding vehicles is replaced with that of predicting the host vehicle. This is valid because two problems can be converted to each other through a simple coordinate transformation. Each model takes the histories of surrounding vehicles and host vehicle within $1s$ at $0.1s$ intervals. The lane information within a $100m$ radius is also used as the network input. Then, each model predicts the future trajectory of the host vehicle for $5s$ at $0.1s$ intervals.

III. PREDICTION MODELS

A. PHYSICS-BASED TRAJECTORY PREDICTION

In this section, we introduce the physics-based motion model as well as a filtering and prediction algorithm under uncertainty.

1) CONSTANT TURN RATE AND Acceleration(CTRA) MODEL

The physics-based model used in this study is CTRA [5], which assumes that the turn rate and acceleration are constant.

The state vector is expressed as follows:

$$\mathbf{x} = (x, y, \theta, v, a, \dot{\psi})^T \tag{1}$$

where x, y indicate the position of the vehicle, θ is the heading angle of the vehicle, v is the velocity, a is the acceleration, and $\dot{\psi}$ is the yaw rate.

The state of the next time step is expressed by

$$\begin{aligned} x_{k+1} &= x_k + \int_0^{\Delta t} v_{x,k}(\tau)\, d\tau \\ &= x_k + \frac{(v_k + a_k \Delta t)\sin(\dot{\psi}_k \Delta t + \theta_k) - v_k \sin\theta_k}{\dot{\psi}_k} \\ &\quad + a_k \frac{\cos(\dot{\psi}_k \Delta t + \theta_k) - \cos\theta_k}{\dot{\psi}_k^2} \end{aligned} \tag{2}$$

$$\begin{aligned} y_{k+1} &= y_k + \int_0^{\Delta t} v_{y,k}(\tau)\, d\tau \\ &= y_k + \frac{v_k \cos\theta_k - (v_k + a_k \Delta t)\cos(\dot{\psi}_k \Delta t + \theta_k)}{\dot{\psi}_k} \\ &\quad + a_k \frac{\sin(\dot{\psi}_k \Delta t + \theta_k) - \sin\theta_k}{\dot{\psi}_k^2} \end{aligned} \tag{3}$$

$$\theta_{k+1} = \theta_k + \dot{\psi}_k \Delta t \tag{4}$$

$$v_{k+1} = v_k + a_k \Delta t \tag{5}$$

$$a_{k+1} = a_k \tag{6}$$

$$\dot{\psi}_{k+1} = \dot{\psi}_k \tag{7}$$

where Δt is the prediction time interval and the subscript k is time step.

2) TRAJECTORY PREDICTION UNDER UNCERTAINTY

The state space equation considering the process noise is expressed as follows:

$$\mathbf{x}_{k+1} = \mathbf{f}_k(\mathbf{x}_k) + \mathbf{w}_k \tag{8}$$

$$\mathbf{y}_k = \mathbf{h}_k(\mathbf{x}_k) + \mathbf{r}_k \tag{9}$$

$$\mathbf{w}_k = [w_x, w_y, w_\theta, w_v, w_a, w_{\dot{\psi}}]^T \tag{10}$$

$$\mathbf{r}_k = [r_x, r_y, r_\theta, r_v]^T \tag{11}$$

where $\mathbf{w}_k$ and $\mathbf{r}_k$ are system noise and observation noise, respectively, both defined as the Gaussian noise.

To solve the nonlinear problem, Unscented Kalman Filter (UKF) is utilized in our work [24]. Unscented transform (UT) is used to consider the uncertainty in the nonlinear dynamic prediction model. A fixed number of sigma points are chosen from the original distribution to estimate the transformed distribution. The UT process is utilized with the motion model to perform the trajectory prediction task considering uncertainty in (8).

B. MANEUVER-BASED TRAJECTORY PREDICTION

In this section, we first introduce trajectory prediction in both the longitudinal and lateral directions in Frenet Coordinates. Then, the intention prediction for selecting one route among several candidates is explained.

1) TRAJECTORY PREDICTION

The longitudinal position prediction along the road is divided into two methods depending on the presence of a lead vehicle. The lead vehicle is a vehicle on the same lane as the host vehicle, within a certain distance. If there is no lead vehicle, the longitudinal position along the road is predicted using the discrete Wiener process acceleration model [11], [25], given by

$$\mathbf{x}_{lon} = (x_{lon}, v_{lon}, a_{lon})^T \tag{12}$$

$$\mathbf{x}_{lon,k+1} = A\mathbf{x}_{lon,k} + Bw_{lon} \tag{13}$$

$$A = \begin{pmatrix} 1 & \Delta t & \frac{1}{2}\Delta t^2 \\ 0 & 1 & \Delta t \\ 0 & 0 & 1 \end{pmatrix} B = \begin{pmatrix} \frac{1}{2}\Delta t^2 \\ \Delta t \\ 1 \end{pmatrix} \tag{14}$$

where Δt is the time interval, the model state $\mathbf{x}_{lon}$ includes longitudinal position x_{lon}, longitudinal velocity v_{lon}, longitudinal acceleration a_{lon}, and w_{lon} indicates the process noise scalar. The covariance matrix of the process noise multiplied by the gain is given by

$$\begin{aligned} Q_k &= B\sigma^2_{\Delta a_{lon}} B^T \\ &= \begin{pmatrix} \frac{1}{4}\Delta t^4 & \frac{1}{2}\Delta t^3 & \frac{1}{2}\Delta t^2 \\ \frac{1}{2}\Delta t^3 & \Delta t^2 & \Delta t \\ \frac{1}{2}\Delta t^2 & \Delta t & 1 \end{pmatrix} \sigma^2_{\Delta a_{lon}} \end{aligned} \tag{15}$$

Thus, the predicted acceleration of the longitudinal model is normally distributed around the current acceleration, and the variance increases linearly, which indicates that the uncertainty of the acceleration profile will increase in the future. If there is a leading vehicle, a_{lon} in the Wiener process acceleration model is replaced by a desired acceleration derived from the constant time gap policy (CTG) of the ACC, given by [26]

$$\dot{e}_{lon} = \dot{x}_{lon,host} - \dot{x}_{lon,lead} \tag{16}$$

$$\delta = x_{lon,host} - x_{lon,lead} + L \tag{17}$$

$$a_{des} = -\frac{1}{h}(\dot{e}_{lon} + \lambda\delta) \tag{18}$$

where h is the time gap, L is the length of the leading vehicle, and λ is the value that adjusts the rate of convergence that makes the error of δ zero. The size of λ is directly proportional to the speed of its convergence. In this step, the velocity of the leading vehicle is considered to maintain the current velocity during the future step.

The lateral position of the vehicle along the road is predicted through the Ornstein-Uhlenbeck process [25] as follows:

$$\dot{y}_{lat}(t) = \alpha(u - y_{lat}(t)) + w_c(t), \quad \alpha > 0 \tag{19}$$

where $y_{lat}(t)$ indicates the lateral position, u is the constant input scalar that shifts the long-term mean, w_c is the Gaussian white noise, α is a value that affects how quickly a vehicle

that is currently not in the middle of the lane will return to the middle of the lane, and $w_c(t)$ is a zero-mean white Gaussian noise process with autocorrelation function as follows:

$$[w_c(t)w_c(t+\tau)] = 2\alpha\sigma_{lat}^2\delta(\tau) \tag{20}$$

An exponentially decaying autocovariance function of $y_{lat}(t)$ is given by

$$[(y_{lat}(t) - \bar{y}_{lat}(t))(y_{lat}(t+\tau) - \bar{y}_{lat}(t+\tau))] = \sigma_{lat}^2 e^{-\alpha|\tau|}. \tag{21}$$

The process in (19) is discretized via a zero-order hold, resulting in

$$y_{lat,k+1} = e^{-\alpha\Delta t}y_{lat,k} + (1 - e^{-\alpha\Delta t})u + w_{lat} \tag{22}$$

$$w_{lat} = \sigma_{lat}^2(1 - e^{-2\alpha\Delta t}) \tag{23}$$

where $\bar{y}_{lat}(\cdot) = (y_{lat}(\cdot))$ and σ_{lat}^2 is the limit of variance which is related to the lane width that prevents the lateral position prediction from deviating significantly from the target lane.

2) INTENTION PREDICTION

Among the trajectory candidates along the road candidates, one optimal maneuver is selected as the final trajectory in a maneuver-based prediction. In order to select an optimal one, the intention is predicted using dynamic time warping (DTW) [27], [28]. DTW measures the temporal changes of two trajectories that do not necessarily have the same length.

We assume the driving intention is to pursue some goals in the intersection, such as lane keeping, turning left and right. The roads that corresponded to the stated intent are set as the reference path. The combined longitudinal and lateral trajectories calculated in III-B1 along the reference path in the Frenet coordinates are transformed to Cartesian coordinates, resulting in the reference trajectories. The trajectory history of the host vehicle is compared with the reference trajectories using the DTW algorithm. Then, the trajectory with the smallest cost is set as the current intention of the host vehicle.

C. LEARNING-BASED TRAJECTORY PREDICTION

1) NETWORK ARCHITECTURE

In this study, we focused on improving the performance using the hybrid model rather than emphasizing the performance of the network model itself. Therefore, a simple network model Resnet18 [29] with an additional fully connected layer, as shown in Fig. 2, is used. The input to the network model is a rasterized image that includes the trajectory histories of the host and surrounding vehicles, and road shape information, which are shown in Fig. 3a, 3b, and 3c, respectively. The Resnet18 layer compresses the input image and generates a vector containing the input information. The fully connected layer reduces this vector and reshapes it to size [50, 4], which indicates the number of future steps and output features (two means and two variances), respectively.

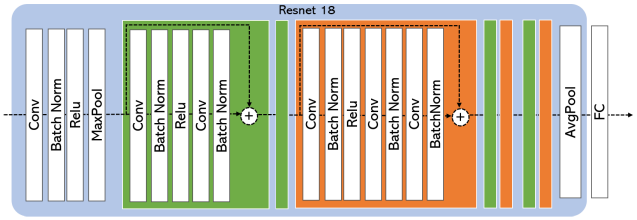

FIGURE 2. Network architecture.

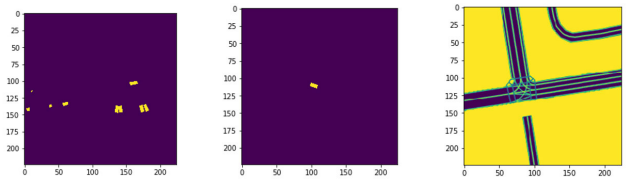

FIGURE 3. Example of the rasterized image. (a) represents surrounding vehicles at a specific time step, (b) shows the host vehicle and (c) is road information.

2) DEEP ENSEMBLE

In order to integrate each model into the hybrid model, the uncertainty of the positions is needed. Physics- and maneuver-based models generate uncertainty using the method described in Section III-A and B, whereas the learning-based model yields uncertainty as a network output. There are many methods for obtaining uncertainty using a deep learning technique. Bayesian deep learning [30], which learns a distribution of weights, is one of the generally used methods. However, this method requires significant changes and more computation than non-Bayesian neural networks. A Bayesian approximation using dropout [31] is introduced to address this problem. This method has the same effect as using multiple models through dropout and the uncertainty can be calculated using the results from each model. The deep ensemble [32] used in this study is a non-Bayesian method and is known to show better uncertainty estimation performance than the dropout method. The deep ensemble treats each model as a mixture model and combines the prediction results as described in Equation (24)

$$p(x) = M^{-1}\sum_{m}^{M}\mathcal{N}(\mu_{\theta_m}(x),\ \sigma_{\theta_m}^2(x)) \tag{24}$$

where M is the number of ensemble models of the same structure with different initializations.

For regression problems, the deep ensemble predicts a mixture of Gaussian distributions where the mean and variance are represented by Equations 25 and 26, respectively.

$$\mu_*(x) = M^{-1}\sum_{m}^{M}\mu_{\theta_m}(x) \tag{25}$$

$$\sigma_*^2(x) = M^{-1}\sum_{m}^{M}(\sigma_{\theta_m}^2(x) + \mu_{\theta_m}^2(x)) - \mu_*^2(x) \tag{26}$$

TABLE 1. Information of sampled dataset.

	Training set	Test set
# of the locations	5	2
Type of intersection	four-way	four-way (severe curvature) three-way
Distance(m)	50	50
# of the data	931,180	195,584
Sample 1	263,159	67,127
Sample 2	419,155	128,457
Sample 3	115,526	-
Sample 4	117,106	-
Sample 5	16,234	-

IV. INTEGRATED TRAJECTORY PREDICTION

The prediction results of the three models are used to generate the final future trajectory. This process comprises of two steps. The first step is to decide whether to use the hybrid model based on the uncertainty of the network output. If the uncertainty is below the threshold, the network output is accepted as the final trajectory without further changes. However, if the uncertainty exceeds the threshold, the next step is performed. In this study, the threshold is set at 1.25 m, where the vehicle begins to cross the lane boundary. In the second step, the integration step, the future trajectory is created using the following equation:

$$x_k = \frac{1}{S}\sum_m \frac{w_{m,k}\cdot t_{m,k}}{\sigma_{m,k}}\mu_{m,k} \tag{27}$$

where x_k is the integrated trajectory at time k, subscript m represents each model, S is the normalization factor, μ and σ indicate the mean and the variance of each model and the constant weights w are the variables used to scale the uncertainty of each model. These values make the average magnitude of uncertainty of the three models similar to each other over 1 s known as the valid range of the physics model [33]. These values are determined by comparing the size of uncertainty in each model during the training step. The time-varying weights t are additional weights for the physics-based model. Because the physics-based model degrades after 1 s, we reduce the effect of the physics-model using Equation (28).

$$t_{m,k} = \begin{Bmatrix} \frac{1}{(1+e^{-3(k-1.5)})} & if \ \text{physics-based} \\ 1 & else \end{Bmatrix} \tag{28}$$

V. SCENARIO SIMULATION FOR VALIDATION

A. DATASET FOR SIMULATION

The Lyft l5 dataset [34] is a collection of real-world vehicle driving data containing different types of intersections. It provides road boundary and historical information of road components, and includes tools to convert this information into rasterized images. In this study, we sampled only a few sections near various types of road shapes from the entire dataset to confirmed the performance improvement of the hybrid model in the new environment. The sampled scenarios are intersection situations, and include four-way and three-way situations, as shown in Figs.4 and 5. The details of the dataset are presented in Table 2. In the training step, the network is trained using only four-way scenarios with similar curvatures. In addition, the four-way scenarios have both turn and straight cases, to prevent the network from learning only the straight cases. The test set consists of three-way scenarios and

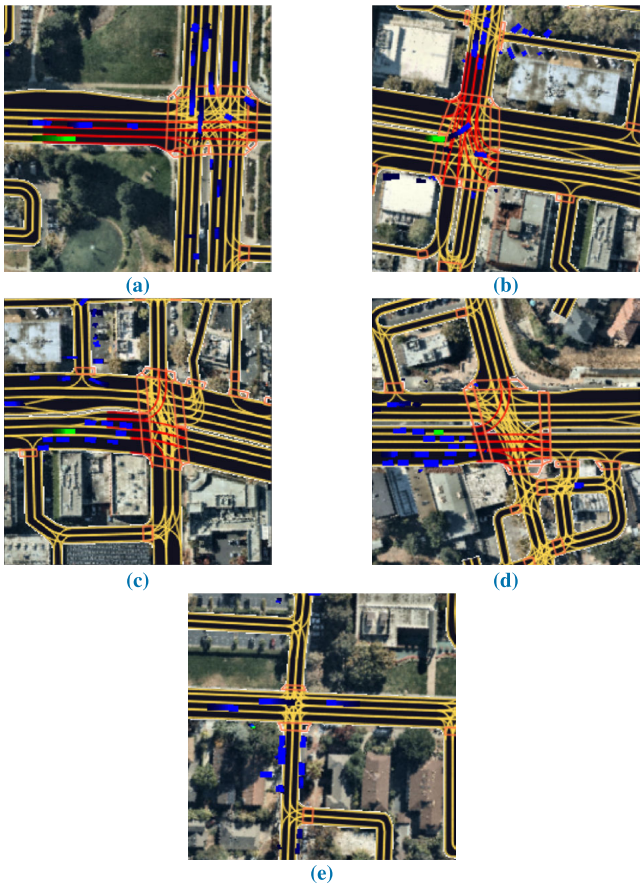

FIGURE 4. Road samples included in the training set. The training set comprised only four-way intersections with similar curvature. The green object represents the host vehicle.

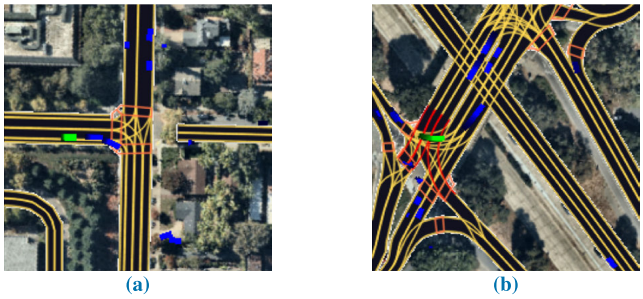

FIGURE 5. Road samples included in the test set. (a) three-way, (b) wavy roads and roads with severe curvature that are not included in the training.

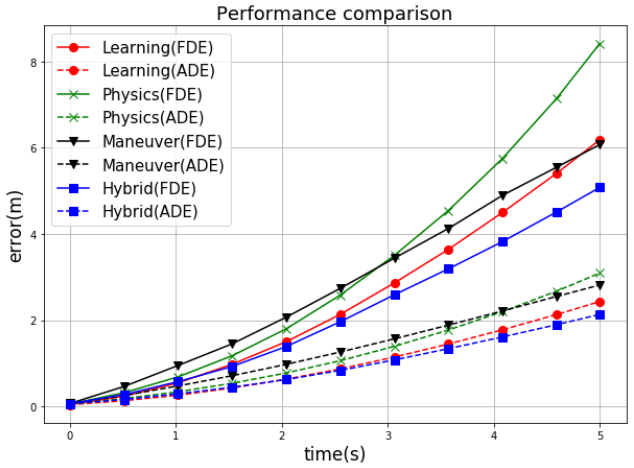

FIGURE 6. Performance comparison results. Solid line and dashed lines represent FDE and ADE, respectively.

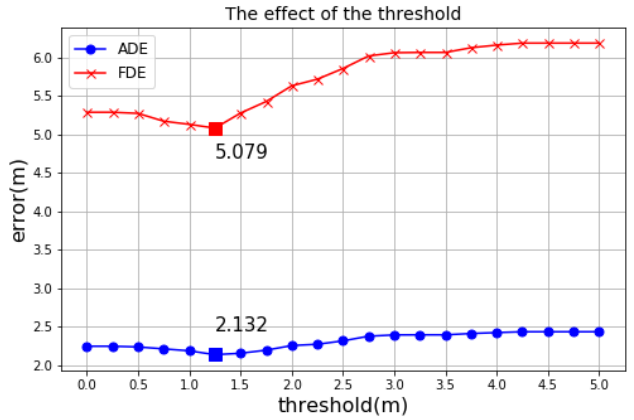

FIGURE 7. Performance comparison according to threshold.

scenarios with wavy shapes and different road curvatures to verify the performance improvement of the hybrid model in the new environment.

B. SIMULATION RESULTS

In this study, the hybrid model and three other models are used for the performance comparison. A comparison was made for the final displacement error (FDE) and the average displacement error (ADE), defined as

$$ADE = \frac{1}{T}\sqrt{\sum_{t}^{T}(x_t - \hat{x}_t)^2 + (y_t - \hat{y}_t)^2} \tag{29}$$

$$FDE = \sqrt{(x_T - \hat{x}_T)^2 + (y_T - \hat{y}_T)^2} \tag{30}$$

Tables 2, 3 and Fig. 6 presents the performance results for each model. The results show that the ADE and FDE of the proposed method are smaller, compared to when only the learning-based method is used. However, the hybrid model shows only a minor performance improvement. This is because the test set contains cases such as a crossroads

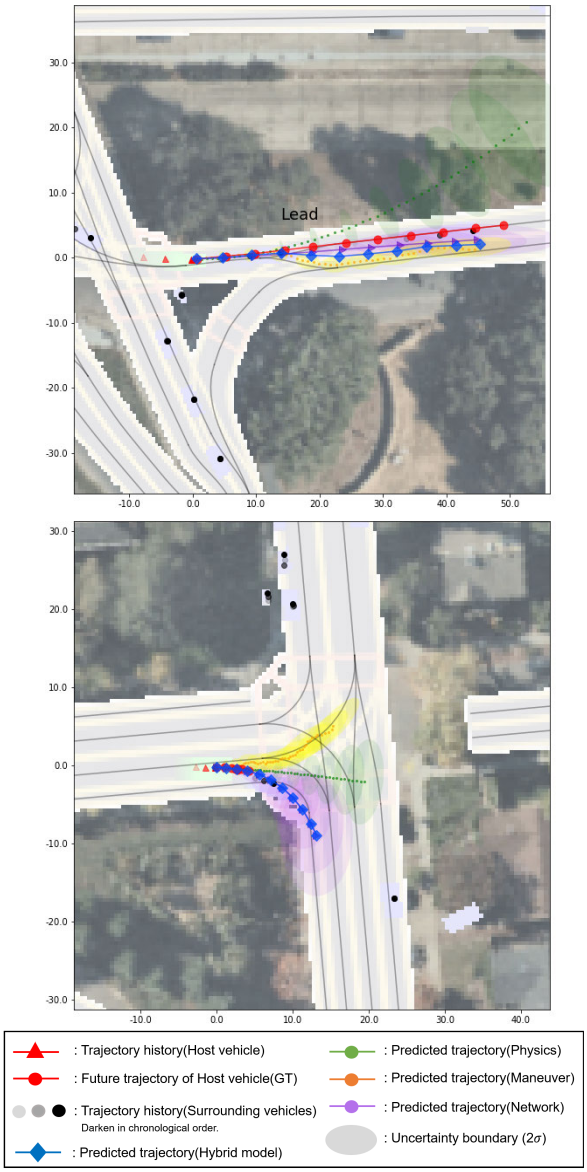

FIGURE 8. Example of wrong maneuver selection. Predicted trajectories for the physics and maneuver models are plotted for 0.1 s intervals and 0.5 s intervals for the remaining trajectories.

TABLE 2. ADE(m).

Prediction horizon (s)	Learning	Physics	Maneuver	Hybrid
1	**0.257**	0.337	0.473	0.289
2	0.629	0.773	0.973	**0.620**
3	1.142	1.391	1.565	**1.076**
4	1.775	2.195	2.212	**1.609**
5	2.430	3.092	2.815	**2.132**

scenario, where it is difficult to determine future maneuvers based on trajectory history alone. In Fig. 8, it can be observed that the host vehicle is approaching the crossroads; however,

FIGURE 9. Qualitative analysis of predictions (a) new road type (b) presence of lead vehicle (c) 3-way intersections.

TABLE 3. FDE(m).

Prediction horizon (s)	Learning	Physics	Maneuver	Hybrid
1	**0.544**	0.682	0.948	0.572
2	1.499	1.798	2.068	**1.386**
3	2.862	3.502	3.437	**2.588**
4	4.497	5.751	4.894	**3.822**
5	6.185	8.419	6.037	**5.079**

its intended direction is not yet known. In this case, incorrect maneuver selection can lead to large errors. Nonetheless, because the future trajectory is predicted directly based on the road shape, the error rate of the proposed model increased slightly as the time step increases. Therefore, it can be seen that the proposed model outperforms the learning-based only model as the time step increases.

We performed additional tests to confirm the influence of the threshold on determining whether or not to use the hybrid model. As shown in Fig. 7, the hybrid model represents the minimum error in terms of both the ADE and FDE, when the threshold is set to 1.25m. Most vehicles drive within a range at which they do not invade other lanes. Therefore, abnormal predictions can be deemed as those exceeding the range of 1.25m, the range at which the vehicle invades another lane.

TABLE 4. Computation times.

Learning	Maneuver	Physics	Integration	Total
0.047 s	0.033 s	0.016 s	0.001 s	**0.097** s

Finally, the real-time performance of proposed model is analyzed. Its average computation time is approximately 0.097 s. The computation times for each model are presented in Table 4. A total time of less than 100ms is reasonable, compared to the typical period of path planning. In addition, the proposed architecture is allowed to change each model; thus, the computation time can be reduced if it is needed.

C. QUALITATIVE ANALYSIS OF PREDICTIONS

In this section, the predicted trajectory is qualitatively analyzed to confirm the validity of the proposed model for representative examples of the test set. Fig. 9 shows three different

scenarios. The first case is when the vehicle encounters a new road shape that is not considered during the training step. Fig. 9(a) shows wavy roads and roads with different curvatures from those in the training dataset. In the upper image, the road shape is wavy; but the network model represented by blue dotted line predicts the future trajectory as a straight line with a lateral uncertainty of 1.5m. The lower image shows the case of a road with more severe curvature than the training data. The network model predicts a less curved trajectory because it learned the distribution of correct answers from the distribution of the training data. In contrast, because the maneuver model represented by the orange dotted line predicts the future trajectory based on the road shape, it was found that the maneuver-based model adapts well to the new types of road shapes. Fig. 9(b) shows the effects of the leading vehicle. After passing an intersection, the vehicle velocity often increases, which makes it difficult to accurately predict the acceleration of future trajectory based solely on the trajectory history. Because the lead vehicle can increase the accuracy of future trajectory predictions by providing a reference to the future velocity profile, the maneuver-based model improves the prediction performance by using an ACC strategy when there is a lead vehicle. At 5 s, it was observed that this strategy reduced the FDE by 18.7%, from 5.66 to 4.60m and the ADE by 16.6%, from 2.35 to 2.00m, compared to when there was no lead vehicle. Fig. 9(c) shows a three-way intersection. In this case, it is found that the performances of the learning-based and the hybrid models are similar. This is because that training was conducted at a four-way intersection with a similar angle to a three-way intersection. Because the network learned to turn left and right at an angle close to the vertical, similar performance could be achieved at a three-way intersection. Overall, these results suggest that the hybrid model, which combines the three models, predicts the future trajectory more effectively than the learning-based model because it considers the shape of the road and movement of surrounding vehicles once more.

VI. CONCLUSION AND FUTURE WORKS

In this study, a hybrid model integrating learning-, physics-, and maneuver-based models is proposed for the trajectory prediction. Because the deep ensemble tends to present large uncertainties for unseen data, the hybrid model determines whether to use the network output solely based on the amount of uncertainty. This method makes it possible to prevent serious accidents that can occur with the unexpected predictions made by the learning-based method in a new environment. The simulation results proves that the proposed method outperforms the learning-based method. Specifically, when there is a road of a different type from the training data or there is a lead vehicle, the performance appears to be improved further. However, in this study, the final trajectory is generated by integrating the three models according to the uncertainty of each model. This method can lead to the problem of predicting the intermediate trajectory when each model predicts multi-branched trajectory and they has a similar magnitude of uncertainty. Therefore, in future work, we will focus on integrating multiple models in a more sophisticated manner. In addition, to cope with complicated situations, such as crossroads, we plan to conduct research toward facilitating the prediction of multiple trajectories, rather than a single one.

REFERENCES

[1] C.-F. Lin, A. G. Ulsoy, and D. J. LeBlanc, "Vehicle dynamics and external disturbance estimation for vehicle path prediction," *IEEE Trans. Control Syst. Technol.*, vol. 8, no. 3, pp. 508–518, May 2000.

[2] M. Brannstrom, E. Coelingh, and J. Sjöberg, "Model-based threat assessment for avoiding arbitrary vehicle collisions," *IEEE Trans. Intell. Transp. Syst.*, vol. 11, no. 3, pp. 658–669, Sep. 2010.

[3] A. Berthelot, A. Tamke, T. Dang, and G. Breuel, "Handling uncertainties in criticality assessment," in *Proc. IEEE Intell. Vehicles Symp. (IV)*, Jun. 2011, pp. 571–576.

[4] A. Polychronopoulos, M. Tsogas, A. J. Amditis, and L. Andreone, "Sensor fusion for predicting vehicles' path for collision avoidance systems," *IEEE Trans. Intell. Transp. Syst.*, vol. 8, no. 3, pp. 549–562, Sep. 2007.

[5] R. Schubert, E. Richter, and G. Wanielik, "Comparison and evaluation of advanced motion models for vehicle tracking," in *Proc. 11th Int. Conf. Inf. Fusion*, Jun. 2008, pp. 1–6.

[6] S. Zernetsch, S. Kohnen, M. Goldhammer, K. Doll, and B. Sick, "Trajectory prediction of cyclists using a physical model and an artificial neural network," in *Proc. IEEE Intell. Vehicles Symp. (IV)*, Jun. 2016, pp. 833–838.

[7] Y. Chen, M. Das, and D. Bajpai, "Improving time-to-collision estimation by IMM based Kalman filter," SAE, Warrendale, PA, USA, Tech. Rep. 2009-01-0162, 2009.

[8] K. Jo, M. Lee, J. Kim, and M. Sunwoo, "Tracking and behavior reasoning of moving vehicles based on roadway geometry constraints," *IEEE Trans. Intell. Transp. Syst.*, vol. 18, no. 2, pp. 460–476, Feb. 2017.

[9] S. Glaser, B. Vanholme, S. Mammar, D. Gruyer, and L. Nouveliere, "Maneuver-based trajectory planning for highly autonomous vehicles on real road with traffic and driver interaction," *IEEE Trans. Intell. Transp. Syst.*, vol. 11, no. 3, pp. 589–606, Sep. 2010.

[10] A. Houenou, P. Bonnifait, V. Cherfaoui, and W. Yao, "Vehicle trajectory prediction based on motion model and maneuver recognition," in *Proc. IEEE/RSJ Int. Conf. Intell. Robots Syst.*, Nov. 2013, pp. 4363–4369.

[11] M. Schreier, V. Willert, and J. Adamy, "An integrated approach to maneuver-based trajectory prediction and criticality assessment in arbitrary road environments," *IEEE Trans. Intell. Transp. Syst.*, vol. 17, no. 10, pp. 2751–2766, Oct. 2016.

[12] G. Xie, H. Gao, L. Qian, B. Huang, K. Li, and J. Wang, "Vehicle trajectory prediction by integrating physics- and maneuver-based approaches using interactive multiple models," *IEEE Trans. Ind. Electron.*, vol. 65, no. 7, pp. 5999–6008, Jul. 2018.

[13] T. Phan-Minh, E. C. Grigore, F. A. Boulton, O. Beijbom, and E. M. Wolff, "CoverNet: Multimodal behavior prediction using trajectory sets," in *Proc. IEEE/CVF Conf. Comput. Vis. Pattern Recognit. (CVPR)*, Jun. 2020, pp. 14074–14083.

[14] Y. Chai, B. Sapp, M. Bansal, and D. Anguelov, "MultiPath: Multiple probabilistic anchor trajectory hypotheses for behavior prediction," 2019, *arXiv:1910.05449*. [Online]. Available: http://arxiv.org/abs/1910.05449

[15] J. Gao, C. Sun, H. Zhao, Y. Shen, D. Anguelov, C. Li, and C. Schmid, "VectorNet: Encoding HD maps and agent dynamics from vectorized representation," in *Proc. IEEE/CVF Conf. Comput. Vis. Pattern Recognit. (CVPR)*, Jun. 2020, pp. 11525–11533.

[16] M. Liang, B. Yang, R. Hu, Y. Chen, R. Liao, S. Feng, and R. Urtasun, "Learning lane graph representations for motion forecasting," in *Proc. Eur. Conf. Comput. Vis.* Cham, Switzerland: Springer, 2020, pp. 541–556.

[17] H. Zhao, J. Gao, T. Lan, C. Sun, B. Sapp, B. Varadarajan, Y. Shen, Y. Shen, Y. Chai, C. Schmid, C. Li, and D. Anguelov, "TNT: Target-driveN trajectory prediction," 2020, *arXiv:2008.08294*. [Online]. Available: http://arxiv.org/abs/2008.08294

[18] H. Kim, D. Kim, G. Kim, J. Cho, and K. Huh, "Multi-head attention based probabilistic vehicle trajectory prediction," in *Proc. IEEE Intell. Vehicles Symp. (IV)*, Oct. 2020, pp. 1720–1725.
[19] Z. Zhao, H. Fang, Z. Jin, and Q. Qiu, "GISNet: Graph-based information sharing network for vehicle trajectory prediction," in *Proc. Int. Joint Conf. Neural Netw. (IJCNN)*, Jul. 2020, pp. 1–7.
[20] A. Sadeghian, V. Kosaraju, A. Sadeghian, N. Hirose, H. Rezatofighi, and S. Savarese, "SoPhie: An attentive GAN for predicting paths compliant to social and physical constraints," in *Proc. IEEE/CVF Conf. Comput. Vis. Pattern Recognit. (CVPR)*, Jun. 2019, pp. 1349–1358.
[21] B. Ivanovic and M. Pavone, "The Trajectron: Probabilistic multi-agent trajectory modeling with dynamic spatiotemporal graphs," in *Proc. IEEE/CVF Int. Conf. Comput. Vis. (ICCV)*, Oct. 2019, pp. 2375–2384.
[22] N. Deo and M. M. Trivedi, "Multi-modal trajectory prediction of surrounding vehicles with maneuver based LSTMs," in *Proc. IEEE Intell. Vehicles Symp. (IV)*, Jun. 2018, pp. 1179–1184.
[23] A. Zyner, S. Worrall, and E. Nebot, "Naturalistic driver intention and path prediction using recurrent neural networks," *IEEE Trans. Intell. Transp. Syst.*, vol. 21, no. 4, pp. 1584–1594, Apr. 2020.
[24] E. A. Wan and R. Van Der Merwe, "The unscented Kalman filter for nonlinear estimation," in *Proc. IEEE Adapt. Syst. Signal Process., Commun., Control Symp.*, Oct. 2000, pp. 153–158.
[25] Y. Bar-Shalom, X. R. Li, and T. Kirubarajan, *Estimation With Applications to Tracking and Navigation: Theory Algorithms and Software*. Hoboken, NJ, USA: Wiley, 2004.
[26] R. Rajamani, *Vehicle Dynamics and Control*. New York, NY, USA: Springer, 2011.
[27] E. J. Keogh and M. J. Pazzani, "Scaling up dynamic time warping for datamining applications," in *Proc. 6th ACM SIGKDD Int. Conf. Knowl. Discovery Data Mining (KDD)*, 2000, pp. 285–289.
[28] Y. Hu, W. Zhan, L. Sun, and M. Tomizuka, "Multi-modal probabilistic prediction of interactive behavior via an interpretable model," in *Proc. IEEE Intell. Vehicles Symp. (IV)*, Jun. 2019, pp. 557–563.
[29] K. He, X. Zhang, S. Ren, and J. Sun, "Deep residual learning for image recognition," in *Proc. IEEE Conf. Comput. Vis. Pattern Recognit.*, Jun. 2016, pp. 770–778.
[30] Y. Gal, *Uncertainty in Deep Learning*, vol. 1, no. 3. Cambridge, U.K.: Univ. Cambridge, 2016, p. 4.
[31] Y. Gal and Z. Ghahramani, "Dropout as a Bayesian approximation: Representing model uncertainty in deep learning," in *Proc. Int. Conf. Mach. Learn.*, 2016, pp. 1050–1059.
[32] B. Lakshminarayanan, A. Pritzel, and C. Blundell, "Simple and scalable predictive uncertainty estimation using deep ensembles," 2016, *arXiv:1612.01474*. [Online]. Available: http://arxiv.org/abs/1612.01474
[33] S. Lefèvre, D. Vasquez, and C. Laugier, "A survey on motion prediction and risk assessment for intelligent vehicles," *Robomech J.*, vol. 1, no. 1, pp. 1–14, Dec. 2014.
[34] J. Houston, G. Zuidhof, L. Bergamini, Y. Ye, L. Chen, A. Jain, S. Omari, V. Iglovikov, and P. Ondruska, "One thousand and one hours: Self-driving motion prediction dataset," 2020, *arXiv:2006.14480*. [Online]. Available: http://arxiv.org/abs/2006.14480

GIHOON KIM received the B.S. degree in automotive engineering from Hanyang University, Seoul, South Korea, in 2017. He is currently pursuing the Ph.D. degree with the Department of Automotive Engineering. His research interests include interaction-aware driving, which is planning the path considering effects to other vehicles from ego vehicle's movement and development of control system for collision avoidance using aggressive-maneuver driving like drift control.

DONGCHAN KIM received the B.S. degree in automotive engineering from Hanyang University, Seoul, South Korea, in 2015. He is currently pursuing the Ph.D. degree with the Department of Automotive Engineering. His research interests include motion planning, trajectory prediction, vehicle state estimation, reinforcement learning, and deep learning.

YOONYONG AHN received the B.S. degree in mechanical and control engineering from Handong Global University, Pohang, South Korea, in 2018. He is currently pursuing the Ph.D. degree with the Department of Automotive Engineering. His research interests include integrated vehicle control, machine learning, and trajectory prediction considering collision risk.

KUNSOO HUH (Member, IEEE) received the Ph.D. degree from the University of Michigan, Ann Arbor, MI, USA, in 1992. He is currently a Professor with the Department of Automotive Engineering, Hanyang University, Seoul, South Korea. His research interests include machine monitoring and control, with emphasis on their applications to vehicular systems. His current research interests include sensor-based active safety systems, V2X-based safety systems, autonomous vehicle control, and AI applications in autonomous vehicle.